Deep–Sea Research I 178 (2021) 103641

Contents lists available at ScienceDirect

Deep-Sea Research Part I

journal homepage: www.elsevier.com/locate/dsri

Feedbacks between hydrodynamics and cold-water coral mound development

Anna-Selma van der Kaaden [a,b,*], Christian Mohn [c], Theo Gerkema [a], Sandra R. Maier [a], Evert de Froe [d], Johan van de Koppel [a], Max Rietkerk [b], Karline Soetaert [a], Dick van Oevelen [a]

[a] NIOZ Royal Netherlands Institute for Sea Research, Department of Estuarine and Delta Systems, PO Box 140, 4400 AC, Yerseke, the Netherlands
[b] Utrecht University, Copernicus Institute of Sustainable Development, Department of Environmental Sciences, PO Box 80.115, 3508 TC, Utrecht, the Netherlands
[c] Aarhus University, Department of Bioscience, Frederiksborgvej 399, 4000, Roskilde, Denmark
[d] NIOZ Royal Netherlands Institute for Sea Research, Department of Ocean Systems, PO Box 59, 1790 AB, Den Burg, the Netherlands

ARTICLE INFO

Keywords:
Baroclinic internal tide
Cold-water coral mounds
Energy conversion rate
Permanent pycnocline
Benthic-pelagic coupling
Feedbacks

ABSTRACT

Cold-water corals rely on currents to transport food towards them and when external conditions are favourable, they can form coral mounds. These structures, which can be over 300 m high, influence the hydrodynamics around the reefs that grow on the mounds, which feeds back to affect coral- and therefore mound-growth. We investigated these feedbacks at the Logachev coral mound province, by running simulations with a 3D hydrodynamic model (Roms-Agrif), using different seafloor bathymetries that represent consecutive stages of mound development. Simulations ranged from a fully smoothened bathymetry without mounds, to a coral mound (Haas mound) at 1.5 times its current size. The effect of mound height on coral growth was investigated by looking at the baroclinic (internal) tide, turbulent energy dissipation, vertical velocities, and horizontal bottom currents. The simulations suggest that with increasing mound height horizontal velocities increase, while turbulent energy dissipation and vertical velocities around the mound foot decrease. This supposedly limits coral growth at the mound foot and hence lateral mound extension in later stages of development. An increase in turbulent energy dissipation and vertical velocities on the mound top and upper flanks, indicates vertical mound growth at all subsequent stages. Our findings of continued vertical mound growth provide an explanation for recently published data on benthic cover from a transect over Haas mound, that show a dominance of live corals on the mound top. We find areas of increased energy conversion rates from the barotropic (surface) to the baroclinic tide on the bathymetry where we artificially eliminated the mounds from (i.e. smoothened bathymetry). Interestingly, these areas overlap with the region where coral mounds are located at present. So, the baroclinic tide is likely an important mechanism in the process of coral mound establishment. Given the relative ease with which the energy conversion rate from the barotropic to the baroclinic tide can be deduced from hydrodynamic model simulations, our results provide opportunities to investigate where coral mounds may be initiated worldwide.

1. Introduction

Cold-water corals rely on currents to transport food towards them, because they are sessile organisms that feed passively on particles flowing past their feeding tentacles (Mortensen, 2001). A logical deduction is then that stronger currents lead to a higher food supply rate and larger coral growth rates. A number of studies have indeed shown that cold-water coral reefs are often found in energetic hydrodynamic regimes (Juva et al., 2020; Mienis et al., 2007; Mohn et al., 2014). When the hydrodynamic conditions are favourable over long time periods, extensive reefs are formed on the seafloor. The reefs trap sediments (de Haas et al., 2009; Dorschel et al., 2005) by baffling currents within their complex three-dimensional structures (Huvenne et al., 2009; Mienis et al., 2019). Where reef growth and sedimentation within these reefs exceed ambient sedimentation rates, cold-water coral reefs can form coral mounds (van der Land et al., 2014).

Studies on the geological history of coral mounds also underline the importance of a strong current regime for coral reef growth, as coral

* Corresponding author. NIOZ Royal Netherlands Institute for Sea Research, Department of Estuarine and Delta Systems, PO Box 140, 4400 AC, Yerseke, the Netherlands.
E-mail address: anna.van.der.kaaden@nioz.nl (A.-S. van der Kaaden).

https://doi.org/10.1016/j.dsr.2021.103641
Received 11 March 2021; Received in revised form 29 September 2021; Accepted 4 October 2021
Available online 14 October 2021

extinction events often happened when hydrodynamic conditions became weaker (e.g. Rüggeberg et al., 2007; Dorschel et al., 2005; Matos et al., 2017; Wienberg et al., 2020).

Coral mounds can be tens of meters to over 300 m high (Mienis et al., 2006) and their presence directly influences the hydrodynamics in coral mound regions: The large structures partially block or deflect the (tidal) flow around them (Cyr et al., 2016; Juva et al., 2020), so that internal waves can be generated, amplified, and locally converted to turbulent motions, increasing the rate at which corals encounter suspended food particles (Mienis et al., 2009; Mohn et al., 2014; van Haren et al., 2014). With isopycnal-displacements of 100–200 m (Mienis et al., 2007; Mohn and White, 2007), downward velocities are increased (Mohn et al., 2014) and hydraulic jumps and internal bores emerge over mound slopes during the turn of the tide (Jackson et al., 2012; Legg and Klymak, 2008). Internal waves are also an important mechanism causing vertical mixing (Jackson et al., 2012) and transport of fresh organic matter from higher up in the water column towards the deep reefs (Davies et al., 2009; Duineveld et al., 2007; Findlay et al., 2013; Kenchington et al., 2017).

The control of hydrodynamics on coral- and mound-growth, combined with the impact of the mounds on the hydrodynamics around the reefs, can be considered as a positive feedback mechanism: Corals themselves increase the rate at which they encounter suspended food particles by affecting the hydrodynamics (van der Kaaden et al., 2020).

There are indications that this coupling between hydrodynamics and reef food uptake changes with mound size and even affects the shape of the mounds. At the Logachev coral mound province (SE Rockall bank margin) for instance, most mounds and mound clusters are elongated in the direction of the tidal currents (White et al., 2007). Such alignment to the current direction has also been observed at other locations (e.g. Hebbeln et al., 2014; Correa et al., 2012; Somoza et al., 2014). Also, since most coral mound tops at Logachev are situated around the depth of the permanent pycnocline, it has been hypothesized that the mounds stop growing taller around this depth there (Mienis et al., 2006; Wheeler et al., 2007; White and Dorschel, 2010). In a 2D modelling study Cyr et al. (2016) compared flow over a small and a large protrusion in the area and suggested that this stabilization of the mound top is controlled by the way the mounds grow: vertically when small until they "outgrow" themselves, after which they mainly grow sideways. This finding was supported by observations of large mounds in the area that seemed to be lacking any live corals on the top. However, due to the inherent symmetry implied in a 2D model, the results of Cyr et al. (2016) represent hydrodynamics around an infinitely long ridge rather than a conical mound.

The feedbacks between mound formation, coral growth and hydrodynamics is challenging to investigate, because of the strongly contrasting time-scales on which these processes occur. Coral mounds form over ten-thousands of years and often over several cycles of coral reef development and extinction (Dorschel et al., 2005; Douarin et al., 2014; Eisele et al., 2011; Titschack et al., 2015). Growth of individual corals, in contrast, changes seasonally (Maier et al., 2020), while hydrodynamics vary over hourly, daily, annual, and even geological time-scales (Colin et al., 2019; Frank et al., 2011; Sherwin et al., 2012).

In this study, we investigate the general process of how hydrodynamics change as a coral mound grows and how this feeds back on coral growth. We simulated the hydrodynamics at the Logachev coral mound province using 3D Regional Ocean Modelling Software (Roms-Agrif), starting with simulations on a bathymetry from which all currently existing mounds were smoothed out. Subsequently, we performed runs where we reintroduced a coral mound of a certain height, by modifying the bathymetry such that the mound height represents different stages of coral mound development. Since hydrodynamic (e.g. stratification) and biological (e.g. algal blooms) conditions differ considerably between seasons (Mohn and White, 2007), we performed winter (February) and summer (August) simulations. This model approach allowed us to study the two tightly-linked processes of mound height and local hydrodynamics in isolation of long-term external changes, e.g. in climate and ocean circulation.

2. Study site

2.1. Mound morphology and distribution at Logachev

The Logachev coral mound province is situated on the south-eastern slope of the Rockall Bank, which is a submerged shallow-summit plateau, elongated in SW-NE direction and situated to the northeast of Ireland (Fig. 1). The Rockall Bank is separated from the continent by the Rockall Trough, which is about 3000 m deep at the southern entrance and about 500 m in the northeast, where it is bounded by the Wyville Thomson Ridge.

The Trough is about 1200 km long, of which the Logachev coral mound province constitutes only a small part of about 80 km long. It consists of clusters of mounds, situated between 600 m and 1000 m depth, that are generally elongated, for several kilometres, perpendicular to the depth contours. Two mounds have been used in this study. The 300 m high Haas mound, and the adjacent, smaller Oreo mound (Fig. 1). The foot of Haas mound is located at around 850 m depth and its top around 550 m depth. Oreo mound is situated to the west of Haas mound, with its foot at around 1000 m depth and its top around 860 m depth.

2.2. Hydrodynamic setting in the Rockall Trough

Water masses show a complex circulation in the Rockall Trough. Around the depth of the Logachev coral mounds, Eastern North Atlantic Water (ENAW) enters the Through in the south and exits in the north (Holliday et al., 2000; Johnson et al., 2010; McGrath et al., 2012; Ullgren and White, 2010). Also entering the Trough in the south are Sub-Arctic Intermediate Water (SAIW) and Mediterranean Water (MW) (Johnson et al., 2010; Ullgren and White, 2010), which mix in the Trough, causing mesoscale activity (i.e. eddies at spatial scales of $<$100 km), so that their signature is lost above 53°N (Ullgren and White, 2010). In the north of the Rockall Trough, Wyville Thomson Overflow Water (WTOW) enters from the Wyville Thomson Ridge between 600 m and 1200 m depth and flows southward along the eastern flank of the Rockall Bank. Its signature can be found as far south as 55°N, where it disappears, probably because it leaves the Trough to the west and because of mixing with other water masses (Johnson et al., 2010). Recent observations confirmed a residual current consisting of WTOW in the Logachev coral mound province, flowing from the northeast to the southwest (Schulz et al., 2020).

The surface signature of the barotropic (surface) tides in the region is semi-diurnal (Gerkema, 2019), but the dominant baroclinic (internal) tide at the Rockall Bank has a diurnal character (van Haren et al., 2014). At the latitude of the Rockall Trough (i.e. above the critical latitude of 30°), these diurnal tidal waves are trapped and travel through the Trough as a Kelvin wave with a wavelength of 300 km. They have the topography on their right and induce currents going up and down the northern trough margin (Cyr et al., 2016; Huthnance, 1974; Pingree and Griffiths, 1984).

The permanent pycnocline extends to about 600 m depth in the Rockall Trough and the water column in the upper 600 m is well-mixed in winter (Ellett and Martin, 1973; Holliday et al., 2000; Ullgren and White, 2010). White and Dorschel (2010) argue that the permanent pycnocline is important for coral mound formation, because at this depth enhanced residual and tidal currents have been measured. Furthermore, because current speeds are maximal around the depth of the pycnocline, divergence above and convergence below the pycnocline-depth cause a conveyer belt-like process whereby organic matter is transported towards the benthic boundary layer (White and Dorschel, 2010). This may also increase organic matter transport towards the seabed (Thiem et al., 2006). The seasonal pycnocline extends

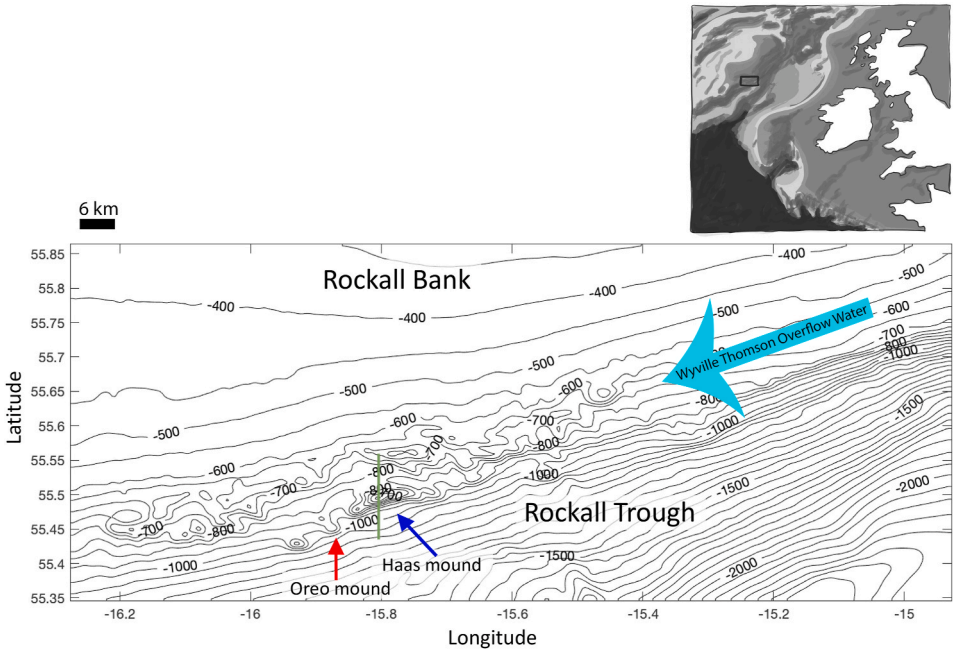

Fig. 1. Contour plot of the Logachev area. The mounds are situated on the southwestern slope of the Rockall Trough. The inset shows that the Rockall Trough is situated west of Ireland. The bathymetry here shows the nested model domain used in the hydrodynamic (Roms) model. The green line depicts the transect used in Fig. 5. At the depth of the mounds, a residual current of Wyville Thomson Overflow Water flows from the northeast to southwest (Schulz et al., 2020). (For interpretation of the references to colour in this figure legend, the reader is referred to the Web version of this article.)

to about 100 m depth (Mienis et al., 2007; White and Dorschel, 2010).

3. Methods

We mimicked mound growth by gradually changing the bathymetry in a number of successive stages. At each of these stages, the hydrodynamics was simulated using a Regional Ocean Modelling Software (Roms-Agrif) model that was validated in a previous study (Mohn et al., 2014). We ran the model for the months of February and August and visualized these winter and summer situations by calculating the Brunt-Väisälä (buoyancy) frequency (N), using the seawater library version 3.3 (©CSIRO 2010). To get insight into how cold-water coral growth is affected by the mound growth stage, we analysed several hydrodynamic parameters that are considered proxies for good coral growth conditions (see section 3.3).

Finally, we make a direct comparison with the present-day favourable conditions for coral growth on Haas mound, by comparing hydrodynamic model results of the present-day Logachev coral mound province with benthic cover on the mound. The data on benthic cover came from an annotated video transect that ran from the upper southern flank to the upper northern flank of Haas mound (Maier et al., 2021).

All computations and pre- and post-processing of the Roms-Agrif files and data were performed in Matlab R2018a.

3.1. Bathymetry

To mimic mound growth, we gradually changed the shape of the bathymetry from no mounds (0 × present size) to 1.5 times the present-day mound size with steps of 1/8 (1/4) for Haas (Oreo) mound, resulting in 13 (7) different stages of coral mound development. Only one (Haas or Oreo) mound was simulated at a time, to avoid interference with the hydrodynamics from the presence of other, nearby mounds. Figures detailing the parameters in side- and top-view are produced for the zero (i.e. "no mound"), 0.5 ("smaller mound"), 1 ("present mound") and 1.5 times ("larger mound") present-day size bathymetries; line graphs show how the hydrodynamic parameters change with mound growth using all 13 (7) stages. As a comparison, all simulations, analyses and calculations were also performed for the unmodified Logachev bathymetry (i.e. all mounds present).

Bathymetric data were derived from Irish National Seabed Survey (INSS), see Mohn et al. (2014) for details. Topographic heights were removed from the original bathymetry by applying a Gaussian filter, leaving behind a smooth continental slope without coral mounds (Fig. 2). The bathymetry of the mounds was isolated by subtracting the actual bathymetry from the smoothened bathymetry and using connected-component labelling. The isolated Haas or Oreo mounds were then modified and subsequently placed back on the "no mounds" bathymetry. To check that the modified bathymetries were not unrealistic, we plotted maximum and mean mound slope (%) against mound height (m) for the modified Haas mound bathymetry and present-day Logachev mounds. The data show a clear height - slope relationship ($R^2 > 0.7$) that the modified mound followed as well (Fig. 3).

3.2. Hydrodynamics

Hydrodynamics was simulated in 3D using the free-surface, hydrostatic equations, 3D Regional Ocean Modelling System with grid refinement (Roms-Agrif). Roms-Agrif solves the equations of motion on

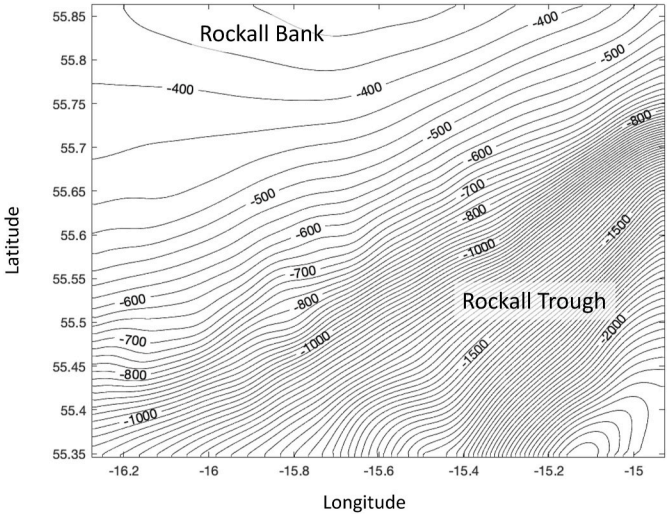

Fig. 2. Smoothened, "no mounds" bathymetry of the Logachev area.

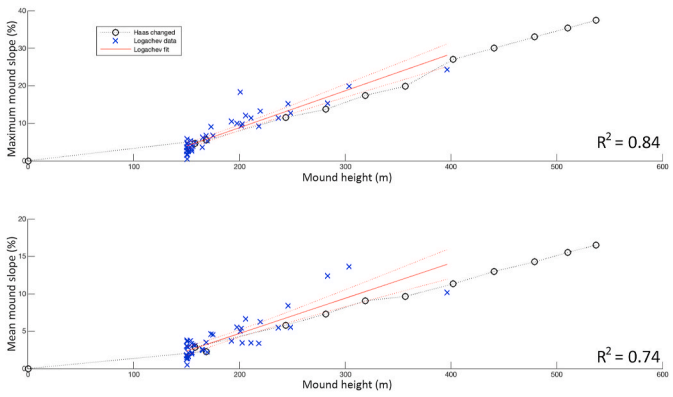

Fig. 3. Maximum (top) and mean (bottom) slope for the present-day Logachev mounds (blue crosses) and for the modified Haas mound (black dots), as a function of mound height (in m). Red line: best fits to the present-day data (solid) with confidence interval (dotted). R^2: variation in the present-day data explained by the fit. (For interpretation of the references to colour in this figure legend, the reader is referred to the Web version of this article.)

a staggered Arakawa-C grid in the horizontal and topography-following coordinates in the vertical (Shchepetkin and McWilliams, 2005). Roms-Agrif employs one-way embedding of multiple grids using the AGRIF package (Adaptive Grid Refinement in Fortran; Penven et al., 2006). Our central model domain covers an area of 85 × 58 km (Fig. 1), with a horizontal resolution of 250 m, nested into a lower resolution (750 m grid size) model grid of 190 × 188 km. The number of vertical topography-following levels is 32 everywhere, with enhanced resolution at the surface and the near-bottom layers. We used an identical setup of a previously described and validated model for the same area and refer to Mohn et al. (2014) for a more detailed description.

The model applies barotropic tidal forcing for 10 major tidal components (M2, N2, S2, K2, K1, O1, P1, Q1, Mf and Mm) along the open lateral boundaries of the lower resolution model, based on the TPXO7 global tidal solution of the Oregon State University (OSU) inverse tidal model (Egbert and Erofeeva, 2002). Water column temperature and salinity were obtained from the monthly World Ocean Atlas (WOA 2005) climatology (i.e. not specific to a certain year). COADS (Comprehensive Ocean-Atmosphere Data Set) data provided atmospheric forcing at the free surface. Water mass properties and currents from the parent grid are transferred as lateral boundary conditions to the child grid at every time step. At the nested grid boundaries, we used a sponge layer of 400 m with a prescribed kinematic viscosity of 40 $m^2\,s^{-1}$ to prevent numerical errors at the edges originating from the modified bathymetry. The model was run for 1 year as a spin-up using climatological forcing and the unmodified bathymetry. The simulations with modified bathymetries were started using the conditions at the end of the spin-up. Model output was then obtained every 6 h in February and August of the climatological year and used for further analysis.

3.3. Derived hydrodynamic parameters

3.3.1. Energy conversion from barotropic to baroclinic tide

When stratified water interacts with the topography, part of the energy from the barotropic (surface) tide is lost to the generation of baroclinic (internal) tides. This conversion from barotropic to baroclinic tidal energy relates to the magnitude of internal tide formation, an important factor causing deep-ocean mixing (de Lavergne et al., 2019; Garrett and Kunze, 2006; Vic et al., 2019).

At Logachev coral mound province, we are interested in the baroclinic K1-tide because it is the dominant component in the area and trapped at the topography. The latter means that instead of travelling away to the interior of the ocean (de Lavergne et al., 2019; Vic et al., 2019), most of the energy is dissipated locally (MacKinnon et al., 2017; Musgrave et al., 2016). To single out the K1 tidal component from the full tidal signal in the model output, we need to calculate the energy conversion without other tidal signals. We therefore calculated the barotropic vertical velocities (W) at the seafloor from depth-averaged horizontal velocities (see appendix A) and fitted them to the K1-tide (see appendix B). Vertical velocities in the other depth layers were obtained by linear interpolation, assuming zero vertical barotropic velocities at the surface. A tidal fit was also produced for the variation of potential density in time, in every layer.

Internal waves are regarded as perturbation of the static equilibrium state. This static equilibrium state, denoted by the subscript "0", is described by the hydrostatic balance:

$$\frac{dp_0}{dz} = -\rho_0 g \tag{1}$$

Density perturbations to this equilibrium state, denoted with a prime, can be introduced as superpositions of their static value:

$$\rho = \rho_0(z) + \rho'(t,x,y,z) \tag{2}$$

In the hypothetical case of a barotropic tide over a horizontal seafloor, water moves essentially horizontal and thus leaves the isopycnals unperturbed. Baroclinic tides (i.e. internal waves at the frequency of the barotropic tide) are created by vertical motions from the barotropic tide induced by a sloping bottom. The energy conversion rate from barotropic to baroclinic tides can then be calculated by multiplying the vertical barotropic velocity (W, in m s^{-1}) by the buoyancy force (b) that acts on these density perturbations, and integrating over one tidal cycle (Gerkema, 2019; Gerkema et al., 2004). The buoyancy force is defined as minus effective gravity:

$$b = -g\rho'/\rho_* \tag{3}$$

with $\rho_* = 1025$ kg m^{-3} and $g = 9.81$ m s^{-2}.

The energy conversion rate is calculated as (Gerkema, 2019; Gerkema et al., 2004):

$$C = -\rho_* bW \tag{4}$$

with: $\ldots = T^{-1}\int_0^T (\ldots)dt$. Here t is time and the averaging interval T is taken as one tidal cycle. C has units of W m-3.

We used the potential density in the calculation (4), because this is the quantity available from the model. This is however equivalent to using the perturbation density ρ' (as in ()4), via b). Introducing C' based on the potential density, we find:

$$C' = -\rho_* - \frac{g}{\rho_*}\rho W \tag{5}$$

$$C' = -\rho_* - \frac{g}{\rho_*}(\rho_0(z) + \rho'(t,x,y,z))W \tag{6}$$

$$C' = -\rho_* - \frac{g}{\rho_*}\rho_0(z)W + -\rho_* - \frac{g}{\rho_*}\rho'(t,x,y,z)W \tag{7}$$

Since $W = 0$ and $\rho_0(z)$ is a constant, the first term on the right side of (5.3) disappears and hence $C' = C$.

We tested whether the 6-hourly resolution of the Roms-output was precise enough to adequately represent the K1-tide, by comparing these results with energy conversion rates obtained using 3 days of hourly output. Both datasets produced qualitatively and quantitatively similar values for energy conversion rates (see Supplementary Figs. S1 and S2), showing that the 6-h resolution suffices for the calculation of these rates.

3.3.2. Turbulent energy dissipation

Turbulence can greatly enhance mixing of particles through the water column and increase the particle encounter rate of feeding corals. The turbulent energy dissipation rate (Thorpe, 2007) describes the

potential of turbulent mixing from current shear of both tidal and mean flow. Following Thorpe (2007) it is estimated as:

$$\varepsilon = (\nu / 2) s_{ij} s_{ij} \quad (8)$$

where ν is the kinematic viscosity and:

$$s_{ij} = \left(\partial u_i / \partial x_j + \partial u_j / \partial x_i\right) \quad (9)$$

where i and j range from 1 to 3 and … indicates the sum of the product of all nine tensors (i.e. $s_{11}s_{11} + s_{12}s_{12} + \ldots + s_{33}s_{33}$). The velocity-components are: $u = u_1$, $v = u_2$, $w = u_3$, for the different directions $x = x_1$, $y = x_2$ and $z = x_3$. The kinematic viscosity is calculated as $\nu = \mu/\rho$, with ρ the actual density, and $\mu = 1.4{\cdot}10^{-3}$ N s m^{-2}.

3.3.3. Vertical velocities

The interaction between coral mounds and waterflow around the mounds can cause downward water motions (Davies et al., 2009; Duineveld et al., 2007; Findlay et al., 2013; Kenchington et al., 2017) that can rapidly transport organic matter from higher up the water column towards the coral reefs. This coupling between the surface and the deep ocean was further investigated using the vertical velocities from the Roms-output between 250 and 300 m depth. We chose this depth range of 250–300 m to be below the seasonal and permanent pycnocline that can hamper vertical mixing.

Vertical velocities are typically directed upward during half of the tidal cycle and downward during the other half. Averaging over the vertical velocities of a perfect (i.e. without a mean flow) tidal cycle, would result in an average of 0 m s^{-1}: the tidal signal is lost during averaging over time. To include both the tidal signal and the effect of the mean flow, we calculated the monthly averages of upward and downward velocities separately.

3.3.4. Horizontal velocities

As the encounter rate of food particles with feeding appendages of passive suspension feeders is related to the current speed, we also analysed horizontal current speed (S), calculated as $S = \sqrt{u^2 + v^2}$ at the bottom layer of the model. Like with vertical velocities, averaging over time of one of the horizontal velocity components would remove the tidal signal. To include both the effect of the tidal signal and mean flow, we calculated S before taking the monthly average.

3.4. Video transect

The benthic cover of a coral mound provides information on the present-day growth conditions of the mound. For example, where live corals prevail, the mound will likely be actively growing, whereas it will not be growing, or even eroding, where dead framework and sediment prevails. Maier et al. (2021) analysed a video transect from the southern to the northern flank of Haas mound, detailing the percentage cover of live reef-building corals, dead coral framework, sediment, large erect sponges, and other macro- or megafauna. We used the data and plotted the coral cover against the hydrodynamic parameters (i.e. energy conversion rate, turbulent energy dissipation rate, vertical velocities, and bottom current speed) from a simulation with the present-day Logachev bathymetry. This allowed us to relate our hydrodynamic parameters to coral mound benthic cover. Values for the hydrodynamic parameters were obtained for every lon-lat coordinate point from the video transect, by selecting the nearest lon-lat coordinate in the Roms-output.

4. Results

4.1. Stratification

The permanent pycnocline, characterized by a maximum buoyancy frequency (N), is located between 700 m and 900 m depth in February (Fig. 5A). Above 600 m depth, the water column is well-mixed in February. The permanent pycnocline is also present in August (Fig. 5B), but mixing above this depth is suppressed by a strong seasonal pycnocline around 100 m depth.

4.2. Energy conversion rate

When there are no mounds, energy is converted to the internal tide on the smooth Rockall Through margin. Interestingly, this band of energy conversion corresponds fairly well with the present-day position of the coral mounds (Fig. 4), especially in February (Fig. 4A).

A transect over Haas mound (see the green transect line in Fig. 1) shows that energy conversion rates are highest near the bottom in February (Fig. 5C–F) and near the bottom and in the seasonal pycnocline in August (Fig. 5K-N). When there is no mound (Fig. 5C and K), little energy is converted to the internal tide, but the region south of where Haas mound formed shows slightly elevated energy conversion rates as compared to the rest of the area. For the smaller Haas mound (Fig. 5D, L), most energy conversion occurs on the southern flank, whereas more energy is converted on the northern flank for the larger mound. No energy is converted at the mound top in all cases, because the barotropic vertical velocities vanish there. On the mound, more energy is converted in August than in February, but in August some of the baroclinic energy is converted back to barotropic energy (i.e. negative values), especially around the seasonal pycnocline and at the mound foot. The energy conversion rate from the baroclinic to barotropic tide (negative values) around the mound foot increases with mound height.

Depth-averaged energy conversion rates over Haas mound increase with mound height (Fig. 6A–D), especially at the northern and southern flanks, in the direction of the tide that travels over the mound in the NW-SE direction.

Energy conversion rates on Oreo mound show a similar pattern as described for the smaller Haas mound stage (see Supplementary Figs. S3 and S4).

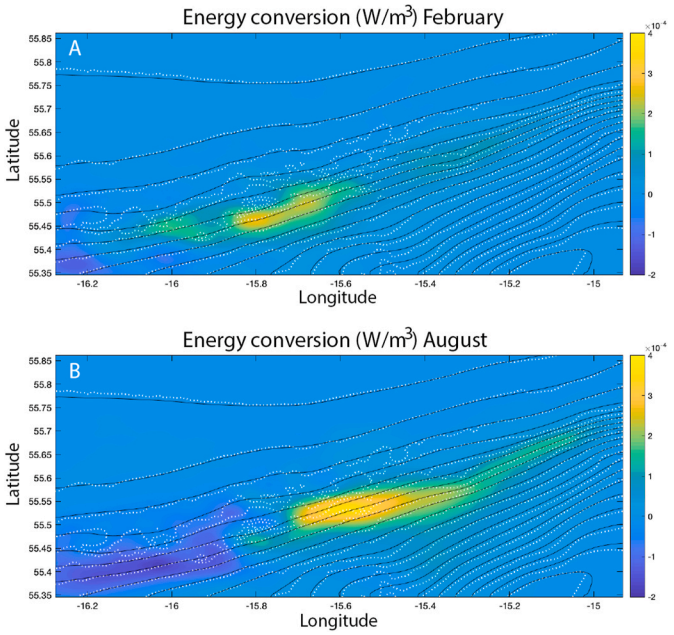

Fig. 4. Top view of monthly averaged energy conversion rates (W/m^3), averaged through the water column for the smoothened Rockall Trough margin bathymetry (i.e. the bathymetry without mounds as shown by the black contour lines). White dotted lines depict the presennt-day position of the mounds.

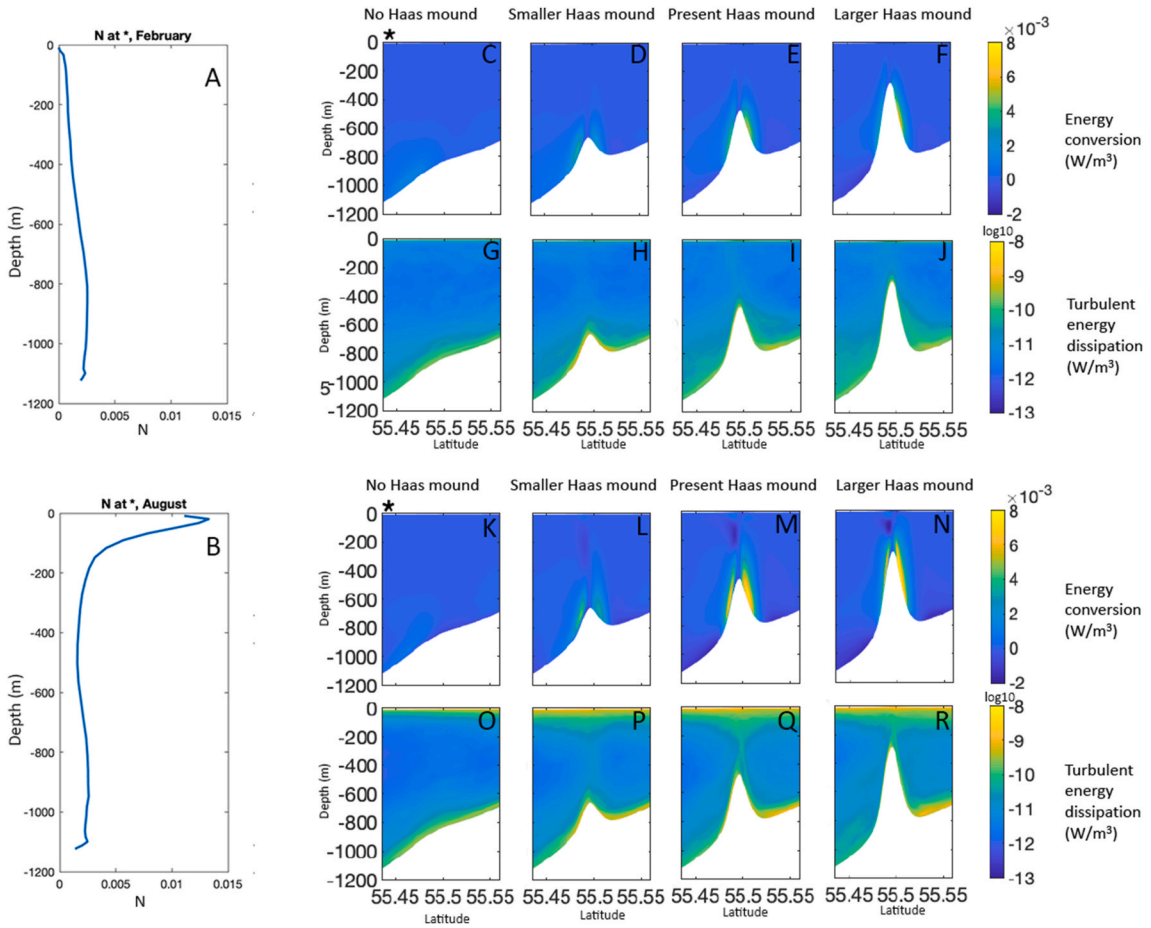

Fig. 5. South to north transect (see the green transect line in Fig. 1) over the tops of different sized Haas mounds. From left to right: no mound, Haas mound at half its present-day size (smaller mound), Haas mound at present size (present mound), and Haas mound at 1.5 times its present size (larger mound). The left two figures show the Brunt-Väisälä (buoyancy) frequency (*N*), in February (A) and August (B), at the deepest part of the transect (left, denoted by * in C and K). The top two rows show the energy conversion rate (W m^{-3}) and turbulent energy dissipation rates (on a $\log_{10}$-scale) in February. The bottom two rows show the same parameters for August. (For interpretation of the references to colour in this figure legend, the reader is referred to the Web version of this article.)

4.3. Turbulent energy dissipation rate

Turbulent energy dissipation rate is highest around the seafloor in February (Fig. 5G–J) and in August around the seafloor and the seasonal pycnocline (Fig. 5O–R). It increases with mound height, especially in the water column and north of the mound at the seafloor.

Depth- and time-averaged turbulent energy dissipation rates over Haas mound are low when no mound is present (Fig. 6E). It increases with mound height at the southern mound flank and to the east of the mound. In August, depth- and time-averaged turbulent energy dissipation rates also increase at some distance from the mound in the north (Fig. 6bH). In February turbulent energy dissipation is lower and decreases on the mound for the larger-mound stage (Fig. 6aH). Turbulent energy dissipation rates on Oreo mound show a similar pattern as described for the smaller Haas mound stage in February (see Supplementary Figs. S3 and S4).

4.4. Vertical velocity

Depth- and time-averaged upward velocities between 250 and 300 m depth, are strongest at the southern foot (northern flank) of the mound in August (February) and become stronger with increasing mound height (Fig. 6J–L). Downward velocities between 250 and 300 m depth are situated around the mound top and western and eastern mound flanks for August and February (Fig. 6N–P). Vertical velocities are generally stronger in August. Again, the results for Oreo mound are similar to the smaller Haas mound stage (see Supplementary Fig. S4).

4.5. Horizontal bottom current speed and direction

Bottom current speeds at Haas mound are elevated compared to the surrounding area, already for the scenario without mounds (Fig. 6Q). They intensify along the southeastern and southwestern flank of Haas mound as the mound grows higher. At the smaller-mound stage bottom current speeds decrease at the northern flank and at the larger-mound stage, bottom current speeds also decrease at the southern flank. This pattern is similar for August and February, but currents are generally stronger in August. Results for Oreo mound are similar to the smaller Haas mound stage (see Supplementary Fig. S4).

4.6. Overall changes with mound height

The relationship between the derived hydrodynamic parameters and mound height was further investigated by averaging them for the area around the mound as depicted in Fig. 6, for all 13 (7) stages for Haas (Oreo) mound (Fig. 7). The curves are plotted against the depth of the mound top, to facilitate comparison with the depth of the permanent pycnocline. We calculated the same hydrodynamic parameters for the entire present-day Logachev coral mound province (i.e. the area on the Rockall Trough margin between 500 m and 1200 m depth).

Energy conversion rates increase with mound height for February and August, but this trend levels off around the depth of the permanent

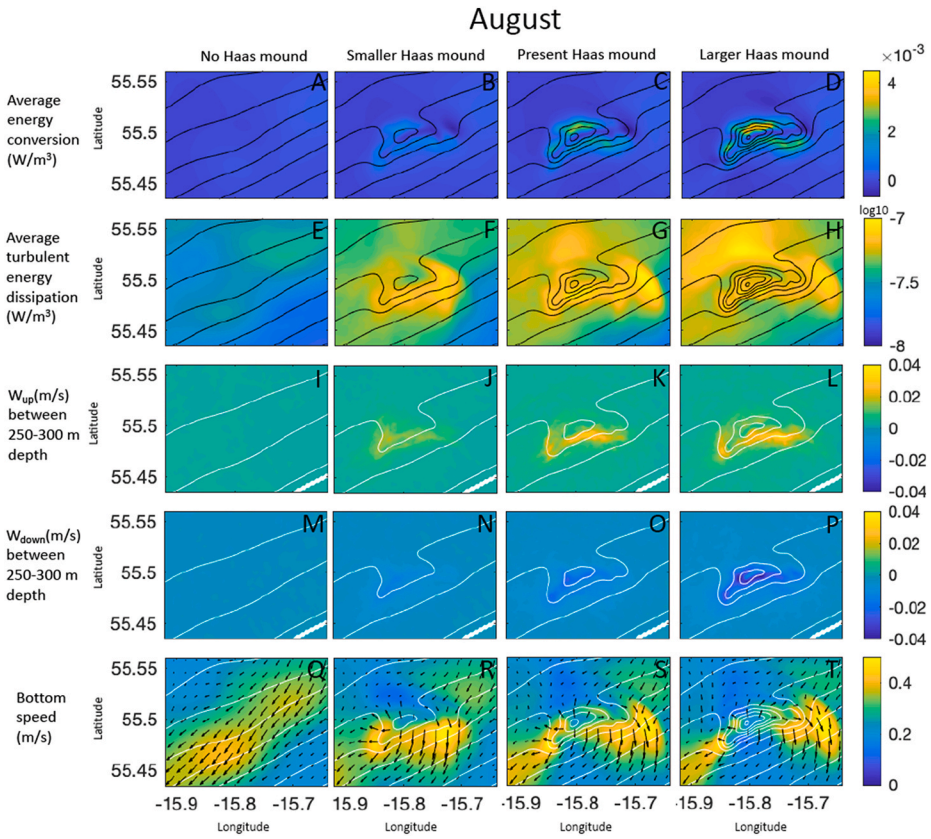

Fig. 6b. From top to bottom: top view of monthly averaged energy conversion rate and turbulent energy dissipation rate (on a $\log_{10}$-scale), averaged through the water column on Haas mound, upward and downward velocities between 250 and 300 m depth, and bottom current speed in August. Depth contour lines are at 100 m level.

pycnocline (600 m) in February (Fig. 7A). The energy conversion rate lies well above the Logachev average (dotted grey line) when no mound is present in February. In August it lies above the Logachev average when the mound is around 100 m tall. Energy conversion rates are higher in February than in August, until the mound top reaches around 550 m depth. Average turbulent energy dissipation rate also increases with mound height and this trend levels off in August, when the mound top reaches around 600 m depth (Fig. 7B). Turbulent energy dissipation rate is higher in August than in February, but lies well above the Logachev average (which is near 0) for both months.

For small mounds, the average vertical velocities between 250 and 300 m depth fall below the Logachev average. The average vertical velocities become stronger with increasing mound height and are above the Logachev average at a mound height larger than 250 m (Fig. 7C). Vertical velocities are generally stronger in August than in February and intensify with increasing mound height, but the increase levels off for up- and downward velocities in both months when the mound top reaches the permanent pycnocline around 600 m depth. Average horizontal bottom currents are also stronger in August than in February (Fig. 7D). Horizontal currents for both months lie above the Logachev average, increase only slightly with mound height in February, and decrease with mound height in August. Horizontal currents over Oreo mound, which is positioned slightly lower on the Rockall Trough margin, are stronger than on Haas mound.

4.7. Coral cover on the present Haas mound

Live coral cover on Haas mound, derived from an annotated S–N video transect in Maier et al. (2021), shows where the present-day living conditions are suitable for coral growth (Fig. 8A). The transect runs from the southern flank to the northern flank, where the mound steeply increases at first, until it reaches its highest point just below 500 m depth (Fig. 8B). The southern flank and especially the mound top have the highest live coral cover. North of the top, the transect shows a relatively flat plateau that is mostly covered with dead coral framework and sediment. At the final 250 m of the transect in the north, the mound descends steeper again, with a small peak in live coral cover after which sediment cover prevails.

Most hydrodynamic parameters are highest around the mound top where live coral cover peaks, except for the depth-averaged energy conversion rate (Fig. 8C). The energy conversion rate is lowest in the transect centre (i.e. on the plateau) and highest on both flanks, with slightly higher values on the northern flank than on the southern flank. Upward velocities (Fig. 8E) are also lowest in the transect centre (i.e. on the plateau). The other parameters are highest in the south and decrease towards the north.

5. Discussion

Most organic matter in the deep sea is transported from the ocean surface. This organic matter supports benthic life, including so-called hotspot ecosystems such as cold-water coral reefs (Cathalot et al., 2015; Rowe and Staresinic, 1979; van Oevelen et al., 2009). We investigated how hydrodynamic parameters that are related to food supply and coral growth, change with mound height and what this implies for coral mound formation. We used several parameters as indicators for good coral growth.

We used the energy conversion rate from the barotropic (surface) to the baroclinic (internal) tide (Gerkema et al., 2004) as an indicator for internal tidal wave activity. Baroclinic tides (i.e. internal waves at the frequency of the barotropic tide) may either radiate away from the topography in internal tidal beams, thereby dissipating most of their

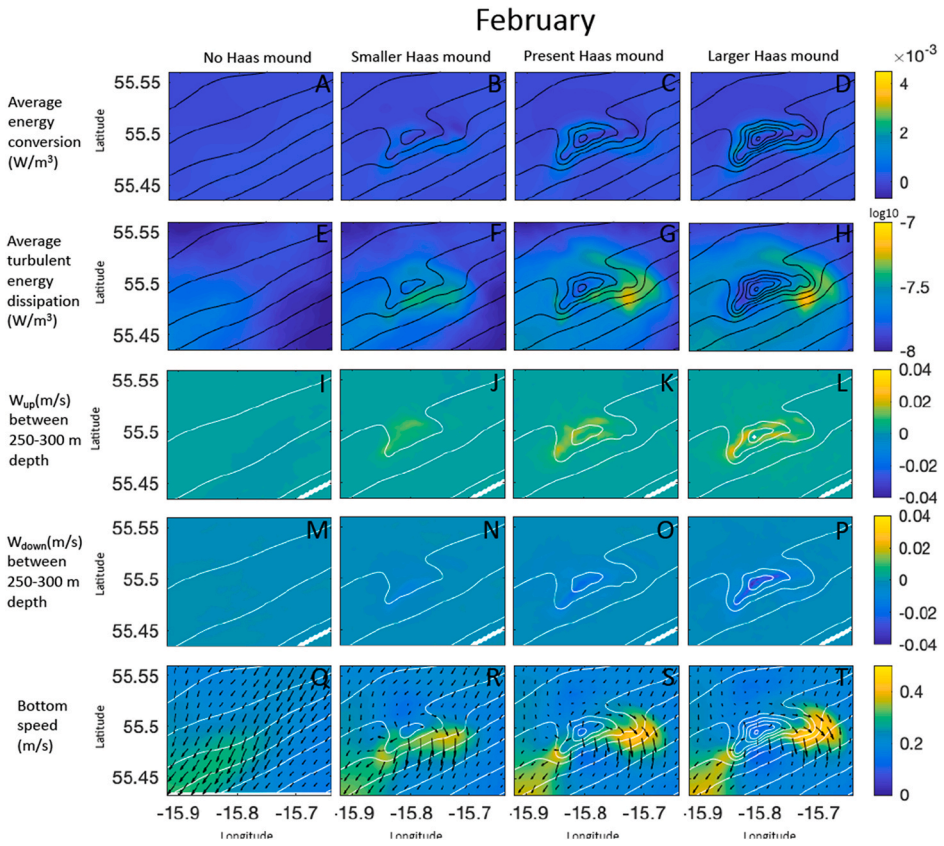

Fig. 6a. From top to bottom: top view of monthly averaged energy conversion rate and turbulent energy dissipation rate (on a $\log_{10}$-scale), averaged through the water column on Haas mound, upward and downward velocities between 250 and 300 m depth, and bottom current speed in February. Depth contour lines are at 100 m level.

energy in the interior of the ocean (de Lavergne et al., 2019; Vic et al., 2019) or be trapped at the topography. When trapped, as is the case for the K1 tide at the Logachev coral mound province, their energy is dissipated locally (MacKinnon et al., 2017; Musgrave et al., 2016). The high energetic regime that comes with these trapped baroclinic tides increases the exchange between surface and deep ocean, enhancing both productivity in the upper layers (Frederiksen et al., 1992) and the concentration of fresh organic matter in deeper water layers (White and Dorschel, 2010).

Other hydrodynamic indicators for favourable food supply are turbulent energy dissipation rate (Thorpe, 2007), vertical velocities between 250 and 300 m depth, and horizontal current speed at the seafloor. Here, we discuss how the hydrodynamic parameters change with different stages of mound development and what the implications are for coral- and mound growth.

5.1. *Baroclinic tides as a driver of coral mound initiation*

How cold-water corals are able to survive in the food-limited deep-sea (Cathalot et al., 2015; Van Engeland et al., 2019), and what determines their spatial distribution (e.g. Eisele et al., 2011; Flögel et al., 2014; Hovland et al., 2012) is still poorly understood. We found that the smoothened Rockall Trough margin bathymetry (i.e. the seafloor without coral mounds) has comparatively high energy conversion rates (Fig. 4) as compared to the surrounding area. This indicates that the mounds seem to have formed at a location with increased baroclinic tidal activity.

Wienberg et al. (2020) noticed, from geological records, that coral mound initiation was linked to internal waves at the other (continental) margin of the Rockall Trough. They attributed the internal wave activity to the transition zone between Mediterranean Outflow Water (MOW) and Eastern North Atlantic Water (ENAW). Wang et al. (2019) made the same connection between coral mound initiation and internal waves, based on geological records in the Alboran Sea. We here show that the correlation between coral mounds and internal waves might be a globally relevant feature, as it seems to be related to the baroclinic tide.

5.2. *Coral food supply increases with mound height*

Internal wave activity has been linked to coral presence (Frederiksen et al., 1992; Wang et al., 2019; Wienberg et al., 2018), because it increases vertical transport of fresh material from higher water towards the deep sea (Jackson et al., 2012; Mohn et al., 2014) and resuspension (Mienis et al., 2009). Our results show highest internal tide activity in winter, when the seasonal pycnocline has not yet developed. Highest activity in winter is not typical of internal tides, but little is still known about the specific nature and dynamics of internal tides above the critical latitude. Wu et al. (2013) found more mixing in winter by the trapped K1 tide in the South China Sea as compared to the summer, which corroborates with our results that the trapped internal K1 tide is more important in February than in August. Furthermore, strong stratification, like the summer stratification, is known to suppresses vertical mixing (Garrett and Kunze, 2006; Kaneda and Ishida, 2000; Legg and Klymak, 2008). In the seasonal pycnocline, internal tides can also scatter into smaller scale waves (Gerkema et al., 2004) and dissipate their energy there, as turbulence (Althaus et al., 2003). This scattering thus also leads to lower vertical mixing and less dissipation around the coral mounds in summer.

Since the other hydrodynamic parameters are less strong in our February than in our August simulation, internal wave activity that is related to the baroclinic tide might be an important food supply mechanism during the winter months. Indeed, it has been suggested that

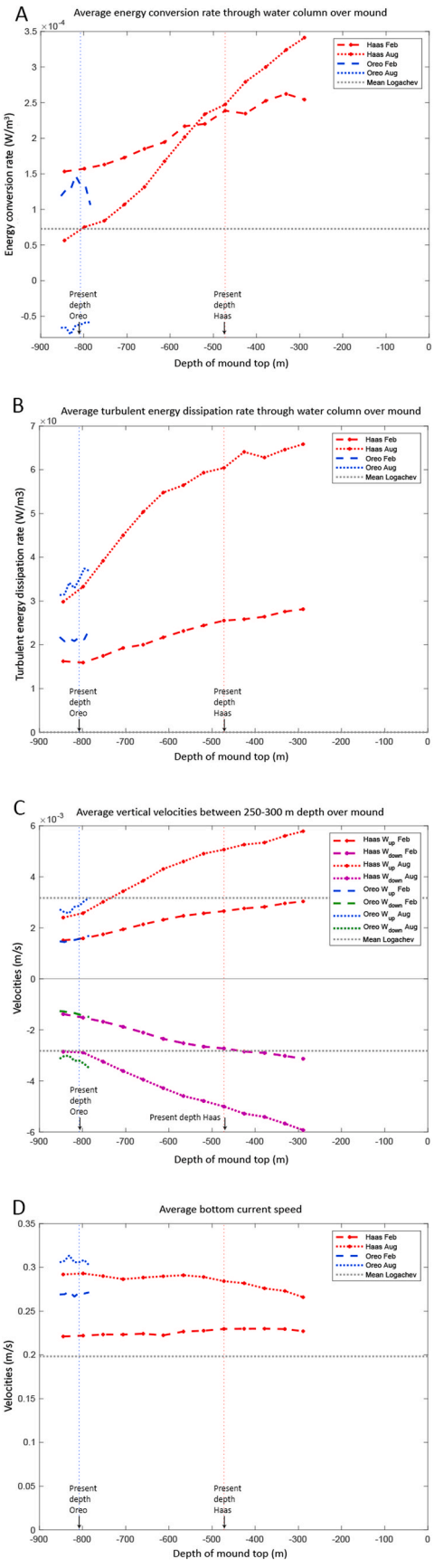

(caption on next column)

Fig. 7. Shown is how average energy conversion rate (A), average turbulent energy dissipation rate (B), average vertical velocities between 250 and 300 m depth (C), and average horizontal speed at the bottom layer (D), change with increasing mound height (i.e. decreasing depth of mound top). Averages were taken over the area around the mound, as depicted in Fig. 6, for the entire water column (A&B), between 250 and 300 m depth (C), or in the bottom layer (D). Vertical dotted lines show the depth at which the tops of the mounds are located at present. The average values for the entire present-day Logachev area are plotted in dotted grey lines.

feeding on resuspended material is an important alternative food source for cold-water corals during winter months (Maier et al., 2020). Furthermore, at Logachev, the spring bloom lasts from February to July (Duineveld et al., 2007) and early in the spring bloom more material is available for downward mixing (Davies et al., 2009; Duineveld et al., 2007; Thiem et al., 2006). So, the baroclinic tide might be important for resuspension and for mixing down of fresh material early in the spring bloom. Since we found that the energy conversion from barotropic to baroclinic tide increases with mound height (Fig. 7A), internal tidal waves are likely an important and consistent food supply mechanism throughout the mound formation process.

Turbulent energy dissipation rate and vertical velocities between 250 and 300 m depth intensify as the mound grows higher (Fig. 7C and D), whereas horizontal currents decrease (August) or change little (February) with mound height (Fig. 7E). This suggests that, with increasing mound height, the flow around a mound becomes more turbulent, with enhanced vertical transport, but with reduced horizontal transport. Turbulence and vertical motions throughout the water column around the mound, stimulate downward transport of fresher food sources from higher up the water column towards the reefs (Soetaert et al., 2016). The observed increase in turbulence and vertical motions in our simulations suggests that the corals on the mounds benefit from the enhanced vertical food supply, irrespective of the reduced horizontal current velocities. Interestingly, the mounds affect the vertical velocities between 250 and 300 m depth already when they are only several tens of meters high. This suggests that coral reefs/mounds can affect benthic-pelagic coupling already from an early stage.

Sessile, passive suspension feeders such as corals rely on currents to transport food towards them, but the idea that passive suspension feeders always benefit from stronger (horizontal) currents is by no means certain (Rubenstein and Koehl, 1977). Experiments show that corals capture food more efficiently and effectively at weak flow conditions below 7 cm s^{-1} (Orejas et al., 2016; Purser et al., 2010), modelling experiments show an optimum ambient flow for food capture between 10 and 30 cm s^{-1} (Hennige et al., submitted) and field evidence showed that more corals live within lower flow conditions and that live corals did not directly face the prevailing current (Lim et al., 2020). Horizontal flows might also be less suited to designate optimal coral reef conditions than vertical flows and turbulence, because food depletion generally occurs downstream of reefs (Wagner et al., 2011).

Tidal downwelling is a known phenomenon around cold-water coral mounds (Davies et al., 2009; Frederiksen et al., 1992) and a previous study observed tidally induced organic matter transport towards Haas mound when simulating organic matter transport (Soetaert et al., 2016). Considering also that organisms living on higher mounds can feed higher in the water column, where organic matter concentration and quality is higher, it can be concluded that the food supply towards organisms living on a coral mound increases with mound height.

Our results for Oreo mound were similar to our results for the smaller Haas mound stage (see supplementary information), which suggests that the results are not typical for the shape of Haas mound, but might be a more general feature of coral mounds at the south-eastern slope of the Rockall Bank. So, in the next section (5.3), we will make some inferences about mound formation at the south-eastern slope of the Rockall Bank.

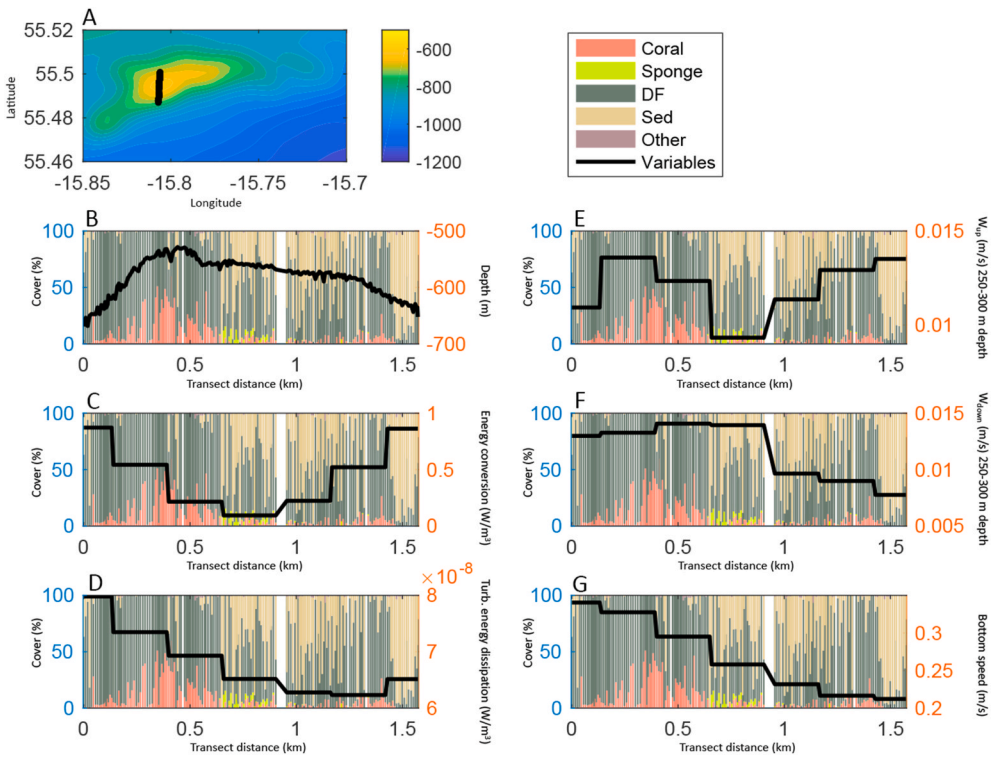

Fig. 8. Data on live coral ('Coral'), sponge, dead coral framework ('DF'), and sediment ('Sed') cover on a South (left) to North (right) transect over Haas mound (A). Benthic cover data from Maier et al. (2021) is plotted as bars with percentage cover on the left y-axis. Panels show different variables along the transect. B: depth in m as measured by the ROV. C: energy conversion rate (W/m^3). D: turbulent energy dissipation (W/m^3). E: upward velocities between 250 and 300 m depth (m/s). F: downward velocities between 250 and 300 m depth (m/s). G: horizontal bottom current speed (m/s). For modelled variables (panels C–G) the mean of February and August is shown.

5.3. *No indications for a negative feedback limiting mound height*

van der Kaaden et al. (2020) proposed that mound formation is subject to spatial feedbacks: positive feedbacks on a coral mound stimulate coral growth, and thereby mound growth, while negative feedbacks hamper lateral mound expansion. Our results show that turbulent energy dissipation rate and vertical velocities become stronger with mound height. Furthermore, horizontal currents decrease markedly to the north of the mound at an early stage of mound growth, possibly leading to a sediment infill as observed by Mienis et al. (2006). Horizontal currents increase at the eastern and western foot and flank as the mound grows higher. This implies that especially the southern mound flank is favourable for coral growth on smaller mounds, suggesting mound expansion in that direction. This could explain why most Logachev coral mounds are elongated in that direction (Mienis et al., 2006). At present, more life coral is observed at the southern than northern upper-flank (Fig. 8), also suggesting mound expansion towards the south.

If the main food supply is due to vertical mixing, our results further imply that the top of Haas mound at and above its present size becomes more favourable for mound growth, as the mound grows higher. This is in line with the present-day Haas mound cover of live corals on the top and upper southern flank (Fig. 8). However, if the main food source would come from lateral transport, horizontal currents, which are more pronounced at the eastern and western flanks would pinpoint these areas to become more favourable with mound growth.

Cold-water corals have variable food sources from pelagic origin (Maier et al., 2019), but also resuspended material and migrating zooplankton (Duineveld et al., 2007; Maier et al., 2020; Van Engeland et al., 2019). The supply of these food sources towards the corals is stimulated especially by high vertical velocities, turbulence and internal waves and most likely intermediate horizontal currents (section 5.2). Therefore, it seems that coral growth is stimulated at the mound top and upper flanks as the coral mound grows higher, which is at least true for the present-day Haas mound (Fig. 8). De Clippele et al. (2019) also reports low (i.e. 0.01–1.71%) live coral cover on the lower east and west flanks of the present-day Haas mound. This suggests that lateral mound growth prevails during the earlier stages of mound formation, and as the mounds grow higher and coral growth is stimulated closer to or on the mound top, vertical growth would be more prominent during all subsequent stages. Consequently, we expect the mound slope to increase with mound height, which can indeed be seen for the present-day Logachev mounds (Fig. 3).

All this leaves the question of why most mound tops are situated around similar depths, just above the permanent pycnocline in the Logachev area (White et al., 2007). White and Dorschel (2010) argue that below the permanent pycnocline, cold-water coral reefs benefit from nutritious water that is transported downward, whereas above the permanent pycnocline the transport is mainly upward. A shift from downward to upward transport with increasing mound height cannot be seen in our results, because both upward and downward velocities increase equally with mound height (Fig. 7C). Furthermore, when the mound breaches through the permanent pycnocline, it is itself situated in these more nutritious waters. Stratification is known to limit vertical water motions, preventing vertical mixing of nutritious water, but this would hamper mound growth already before the mound tops reach the permanent pycnocline. Thus, in our interpretation, the permanent pycnocline is unlikely to limit coral growth, unless coral mounds need large, local vertical water motions to grow, but as of yet there is no evidence to support this latter idea.

Hydraulic drag (causing mound erosion) has been used to explain mound size at the other (continental) Rockall Trough margin (O'Reilly et al., 2003), but is unlikely to limit vertical mound growth at Logachev: hydraulic drag is proportional to the current speed and turbulent flow squared and would thus be expected especially around the eastern, western, and northern mound foot, posing another possible negative feedback around the foot, but not for growth of the mound top.

Another solution to the question of why most tops are situated at similar depth may be that the flow around the mound top becomes less favourable as the structure grows from a situation of partially blocked flow with vertical motions, towards a situation with complete flow blocking and horizontal motions (Cyr et al., 2016; Juva et al., 2020).

Although our results show a slight levelling off of the increasing trend in vertical velocities (Fig. 7C), vertical velocities generally increase whereas horizontal currents decrease (Fig. 7D). Furthermore, this process, which suggests a mechanism that is intrinsic of coral mound growth, would be related to the mound height. However, the Logachev mounds differ in height since their tops are situated around the same depth, while their foots are situated at different depths. It seems more likely that not intrinsic, but external factors are limiting upward mound growth. It could be the result of the mounds growing out of the reach of the Wyville Thomson Overflow Water (as suggested by Schulz et al., 2020). However, the fact that most tops are situated around the same depth can also be reminiscent of past environmental conditions and does not necessarily mean that those mounds stopped growing. The results from the video analysis by Maier et al. (2021) indeed do not provide any evidence that Haas mound stopped growing, since live coral reefs are present at its top.

6. Conclusion

Using a novel combination of mechanistic and conceptual modelling techniques, we studied the interaction between mound height and hydrodynamic conditions at different stages of mound development. Internal waves have been proposed as an important mechanism fostering coral mound growth. We here show that internal tidal waves might be an important mechanism in the process of coral mound initiation and at the same time can provide a stable food supply mechanism during winter for established mounds. Given the relative ease with which the energy conversion rates from the barotropic (surface) to the baroclinic (internal) tide can be inferred from hydrodynamic outputs, this poses an interesting new perspective for cold-water coral research, e.g. to estimate the impact of global environmental changes on cold-water coral occurrence.

Turbulent energy dissipation rate and vertical velocities were shown to increase with mound height, creating a possible positive feedback to mound growth, because these parameters are thought to stimulate coral growth. Assuming that cold-water corals feed optimally in intermediate currents, the western and eastern mound foot become less favourable with mound height, since horizontal bottom currents greatly increase there. This creates a possible negative effect for lateral mound growth. We therefore conclude that mounds mainly grow sideways during early stages of mound development. A positive feedback around the mound top and upper flanks, in combination with a negative feedback around the mound foot, at later stages of mound development, suggests that mounds mainly grow vertically at later stages.

The top of Haas mound being covered with live coral underlines our results that suggest no limiting effect of hydrodynamic parameters on mounds growing higher than the permanent pycnocline, or other intrinsic negative feedbacks limiting mound height. The reason that most mound tops at the Logachev coral mound province are located around similar depths is probably related to external factors, such as the mounds growing out of the reach of the Wyville Thomson Overflow Water mass, or a feature reminiscent of past environmental conditions such as changes in the climate or circulation patterns. In order to more precisely understand coral mound initiation and growth, it is necessary to obtain a better understanding of how coral- and mound growth is linked to certain hydrodynamic parameters.

Funding

This study was made possible through collaboration funding between Utrecht University, the Netherlands, and the Royal Netherlands Institute for Sea Research(NIOZ).

Data availability

All bathymetry-, forcing-, and initial files that are needed to prepare the Roms-Agrif model are available on Zenodo with https://doi.org/10.5281/zenodo.5556805 (van der Kaaden et al., 2021). Individual Roms-Agrif output files in netcdf format can be send on request.

Declaration of competing interest

The authors declare that they have no known competing financial interests or personal relationships that could have appeared to influence the work reported in this paper.

Appendix A. Calculation of vertical velocities

For the calculation of the energy conversion rate from barotropic to baroclinic tide (see eq. (1)), we are looking for the purely barotropic signal (denoted by 'bt') of vertical velocities, at the seafloor (denoted by an asterisk*).

To calculate vertical velocities at the seafloor, we apply the material time derivative ($\frac{d}{dt} = \frac{\partial}{\partial t} + u\frac{\partial}{\partial x} + v\frac{\partial}{\partial y} + w\frac{\partial}{\partial z}$) to $z = -h(x,y)$ at the bottom, to obtain:

$$w_* = -u_*\frac{\partial h}{\partial x} - v_*\frac{\partial h}{\partial y} \tag{A1}$$

The horizontal velocities obtained from the Roms-output contain both a barotropic (*bt*) and baroclinic (*bc*) signal. The velocities can thus be split into a barotropic and baroclinic signal:

$$u_* = u_{*bt} + u_{*bc},\ v_* = v_{*bt} + v_{*bc} \tag{A2}$$

Combining (A1.2) and (A2) it follows that vertical velocities at the bottom are given by:

$$w_* = -(u_{*bt} + u_{*bc})\frac{\partial h}{\partial x} - (v_{*bt} + v_{*bc})\frac{\partial h}{\partial y} \tag{A3}$$

Similarly, we split *w* into a barotropic and baroclinic part, and hence it is natural to assume that:

$$w_{bt*} = -u_{bt*}\frac{\partial h}{\partial x} - v_{bt*}\frac{\partial h}{\partial y} \tag{A4}$$

We assume that the horizontal barotropic velocities do not change with depth:

$$\frac{\partial u_{bt}}{\partial z} = 0\ ,\ \frac{\partial v_{bt}}{\partial z} = 0 \tag{A5.1}$$

Hence, depth averaged horizontal barotropic velocities are the same as their value at the bottom:

$$\overline{u_{bt}} = u_{*bt},\ \overline{v_{bt}} = v_{*bt} \tag{A5.2}$$

where the bar denotes depth averaged values.

To calculate the barotropic vertical velocities at the bottom, we assume that the depth averaged baroclinic horizontal velocities are zero:

$$\overline{u_{bc}} = 0,\ \overline{v_{bc}} = 0 \tag{A5.3}$$

Since the averaged sum of the barotropic and baroclinic component is the same as the sum of the averaged components, we find that the depth-averaged horizontal velocities are the same as the barotropic component at the bottom:

$$\overline{u} = \overline{u_{bt} + u_{bc}} = \overline{u_{bt}} + \overline{u_{bc}} = u_{*bt},\ \overline{v} = \overline{v_{bt} + v_{bc}} = \overline{v_{bt}} + \overline{v_{bc}} = v_{*bt} \tag{A5.4}$$

Using (A4), we can calculate the pure barotropic signal of vertical velocities at the bottom as:

$$-w_{bt^*} = \overline{u}\frac{\partial h}{\partial x} + \overline{v}\frac{\partial h}{\partial y} \tag{A6}$$

The vertical barotropic velocity in the higher layers were obtained by linear interpolation, assuming that it vanishes at the surface; thus we obtain W. To investigate the energy conversion for the dominant barotropic K1-tide we produced tidal fits for the change in vertical velocity and density over time.

Appendix B. Procedure to fit tide

The procedure to obtain a tidal fit for a variable q starts by calculating, for one tidal period T, the constant component $c_0 = T^{-1}\int_0^T q dt$ and then subtracting it from q, to shift the variable so that its mean is at 0. The amplitude (a) and phase (φ) can then be calculated for tidal frequency (σ) as:

$$a = \frac{2}{T}\cdot\sqrt{c_1^2 + c_2^2} \tag{10}$$

$$\varphi = \tan^{-1}\left(-c_2/_{c_1}\right) \tag{11}$$

with: $c_1 = \int_0^T q\cdot\sin(\sigma t)dt$ and $c_2 = \int_0^T q\cdot\cos(\sigma t)dt$ and $\sigma = \sigma_{K1} = 7.2921\cdot10^{-5}$.

Which produces the tidal fit

$$q' = a\cdot\sin(\sigma t - \varphi) \tag{12}$$

Fitted time series were visually inspected for several locations and were judged to be good fits.

Appendix C. Supplementary data

Supplementary data to this article can be found online at https://doi.org/10.1016/j.dsr.2021.103641.

References

Althaus, A.M., Kunze, E., Sanford, T.B., 2003. Internal tide radiation from Mendocino escarpment. J. Phys. Oceanogr. 33, 1510–1527. https://doi.org/10.1175/1520-0485(2003)033<1510:ITRFME>2.0.CO;2.

Cathalot, C., Van Oevelen, D., Cox, T.J.S., Kutti, T., Lavaleye, M., Duineveld, G., Meysman, F.J.R., 2015. Cold-water coral reefs and adjacent sponge grounds: hotspots of benthic respiration and organic carbon cycling in the deep sea. Front. Mar. Sci. 2, 1–12. https://doi.org/10.3389/fmars.2015.00037.

Colin, C., Tisnérat-Laborde, N., Mienis, F., Collart, T., Pons-Branchu, E., Dubois-Dauphin, Q., Frank, N., Dapoigny, A., Ayache, M., Swingedouw, D., Dutay, J.C., Eynaud, F., Debret, M., Blamart, D., Douville, E., 2019. Millennial-scale variations of the Holocene North Atlantic mid-depth gyre inferred from radiocarbon and neodymium isotopes in cold water corals. Quat. Sci. Rev. 211, 93–106. https://doi.org/10.1016/j.quascirev.2019.03.011.

Correa, T.B.S., Eberli, G.P., Grasmueck, M., Reed, J.K., Correa, A.M.S., 2012. Genesis and morphology of cold-water coral ridges in a unidirectional current regime. Mar. Geol. 326–328, 14–27. https://doi.org/10.1016/j.margeo.2012.06.008.

Cyr, F., Van Haren, H., Mienis, F., Duineveld, G., Bourgault, D., 2016. On the influence of cold-water coral mound size on flow hydrodynamics, and vice versa. Geophys. Res. Lett. 43, 1–9. https://doi.org/10.1002/2015GL067038.

Davies, A.J., Duineveld, G.C.A., Lavaleye, M.S.S., Bergman, M.J.N., van Haren, H., Roberts, J.M., 2009. Downwelling and deep-water bottom currents as food supply mechanisms to the cold-water coral Lophelia pertusa (Scleractinia) at the Mingulay Reef complex. Limnol. Oceanogr. 54, 620–629. https://doi.org/10.4319/lo.2009.54.2.0620.

De Clippele, L.H., Huvenne, V.A.I., Molodtsova, T.N., Roberts, J.M., 2019. The diversity and ecological role of non-scleractinian corals (Antipatharia and Alcyonacea) on scleractinian cold-water coral mounds. Front. Mar. Sci. 6, 1–16. https://doi.org/10.3389/fmars.2019.00184.

de Haas, H., Mienis, F., Frank, N., Richter, T.O., Steinacher, R., de Stigter, H., van der Land, C., van Weering, T.C.E., 2009. Morphology and sedimentology of (clustered) cold-water coral mounds at the south Rockall Trough margins, NE Atlantic Ocean. Facies 55, 1–26. https://doi.org/10.1007/s10347-008-0157-1.

de Lavergne, C., Falahat, S., Madec, G., Roquet, F., Nycander, J., Vic, C., 2019. Toward global maps of internal tide energy sinks. Ocean Model. 137, 52–75. https://doi.org/10.1016/j.ocemod.2019.03.010.

Dorschel, B., Hebbeln, D., Ruggeberg, A., Dullo, C., 2005. Carbonate budget of a cold-water coral carbonate mound: propeller Mound, Porcupine Seabight. Int. J. Earth Sci. 96, 73–83. https://doi.org/10.1007/s00531-005-0493-0.

Douarin, M., Sinclair, D.J., Elliot, M., Henry, L.-A., Long, D., Mitchison, F., Roberts, J.M., 2014. Changes in fossil assemblage in sediment cores from Mingulay Reef Complex (NE Atlantic): implications for coral reef build-up. Deep. Res. Part II 99, 286–296. https://doi.org/10.1016/j.dsr2.2013.07.022.

Duineveld, G.C.A., Lavaleye, M.S.S., Bergman, M.J.N., de Stigter, H., Mienis, F., 2007. Trophic structure of a cold-water coral mound community (Rockall Bank, NE Atlantic) in relation to the near-bottom particle supply and current regime. Bull. Mar. Sci. 81, 449–467. https://doi.org/10.1080/17451000.2017.1398404.

Egbert, G.D., Erofeeva, S.Y., 2002. Efficient inverse modeling of barotropic ocean tides. J. Atmos. Ocean. Technol. 19, 183–204. https://doi.org/10.1175/1520-0426(2002)019<0183:EIMOBO>2.0.CO;2.

Eisele, M., Frank, N., Wienberg, C., Hebbeln, D., López Correa, M., Douville, E., Freiwald, A., 2011. Productivity controlled cold-water coral growth periods during the last glacial off Mauritania. Mar. Geol. 280, 143–149. https://doi.org/10.1016/j.margeo.2010.12.007.

Ellett, D.J., Martin, J.H.A., 1973. The physical and chemical oceanography of the Rockall channel. Deep. Res. Oceanogr. Abstr. 20 https://doi.org/10.1016/0011-7471(73)90030-2.

Findlay, H.S., Artioli, Y., Moreno Navas, J., Hennige, S.J., Wicks, L.C., Huvenne, V.A.I., Woodward, E.M.S., Roberts, J.M., 2013. Tidal downwelling and implications for the carbon biogeochemistry of cold-water corals in relation to future ocean acidification and warming. Global Change Biol. 19, 2708–2719. https://doi.org/10.1111/gcb.12256.

Flögel, S., Dullo, W.C., Pfannkuche, O., Kiriakoulakis, K., Rüggeberg, A., 2014. Geochemical and physical constraints for the occurrence of living cold-water corals. Deep. Res. Part II Top. Stud. Oceanogr. 99, 19–26. https://doi.org/10.1016/j.dsr2.2013.06.006.

Frank, N., Freiwald, A., López Correa, M., Wienberg, C., Eisele, M., Hebbeln, D., Van Rooij, D., Henriet, J.P., Colin, C., van Weering, T., de Haas, H., Buhl-Mortensen, P., Roberts, J.M., De Mol, B., Douville, E., Blamart, D., Hatté, C., 2011. Northeastern Atlantic cold-water coral reefs and climate. Geology 39, 743–746. https://doi.org/10.1130/G31825.1.

Frederiksen, R., Jensen, A., Westerberg, H., 1992. The distribution of the scleractinian coral Lophelia pertusa around the Faroe Islands and the relation to internal tidal mixing. Sarsia 77, 157–171. https://doi.org/10.1080/00364827.1992.10413502.

Garrett, C., Kunze, E., 2006. Internal tide generation in the deep ocean. Annu. Rev. Fluid Mech. 39, 57–87. https://doi.org/10.1146/annurev.fluid.39.050905.110227.

Gerkema, T., 2019. An Introduction to Tides. Cambridge University Press. https://doi.org/10.1017/9781316998793.

Gerkema, T., Lam, F.P.A., Maas, L.R.M., 2004. Internal tides in the Bay of Biscay: conversion rates and seasonal effects. Deep. Res. Part II Top. Stud. Oceanogr. 51, 2995–3008. https://doi.org/10.1016/j.dsr2.2004.09.012.

Hebbeln, D., Wienberg, C., Wintersteller, P., Freiwald, A., Becker, M., Beuck, L., Dullo, C., Eberli, G.P., Glogowski, S., Matos, L., Forster, N., Reyes-Bonilla, H., Taviani, M., 2014. Environmental forcing of the Campeche cold-water coral province, southern Gulf of Mexico. Biogeosciences 11, 1799–1815. https://doi.org/10.5194/bg-11-1799-2014.

Holliday, N.P., Pollard, R.T., Read, J.F., Leach, H., 2000. Water mass properties and fluxes in the Rockall Trough, 1975-1998. Deep. Res. Part I Oceanogr. Res. Pap. 47, 1303–1332. https://doi.org/10.1016/S0967-0637(99)00109-0.

Hovland, M., Jensen, S., Indreiten, T., 2012. Unit pockmarks associated with Lophelia coral reefs off mid-Norway : more evidence of control by ' fertilizing ' bottom currents. Geo Mar. Lett. 32, 545–554. https://doi.org/10.1007/s00367-012-0284-0.

Huthnance, J.M., 1974. On the diurnal tidal currents over Rockall Bank. Deep. Res. Oceanogr. Abstr. 21, 23–35. https://doi.org/10.1016/0011-7471(74)90016-3.

Huvenne, V.A.I., Van Rooij, D., De Mol, B., Thierens, M., O'Donnell, R., Foubert, A., 2009. Sediment dynamics and palaeo-environmental context at key stages in the Challenger cold-water coral mound formation: clues from sediment deposits at the mound base. Deep. Res. Part I Oceanogr. Res. Pap. 56, 2263–2280. https://doi.org/10.1016/j.dsr.2009.08.003.

Jackson, C., Da Silva, J., Jeans, G., 2012. The generation of nonlinear internal waves. Oceanography 25, 108–123. https://doi.org/10.5670/oceanog.2011.65.

Johnson, C., Sherwin, T., Smythe-Wright, D., Shimmield, T., Turrel, W., 2010. Wyville Thomson Ridge Overflow water: spatial and temporal distribution in the Rockall Trough. Deep. Res. Part I 57, 1153–1162. https://doi.org/10.1016/j.dsr.2010.07.006.

Juva, K., Flögel, S., Karstensen, J., Linke, P., Dullo, W.-C., 2020. Tidal dynamics control on cold-water coral growth: a high-resolution multivariable study on eastern Atlantic cold-water coral sites. Front. Mar. Sci. 7, 132. https://doi.org/10.3389/FMARS.2020.00132.

Kaneda, Y., Ishida, T., 2000. Suppression of vertical diffusion in strongly stratified turbulence. J. Fluid Mech. 402, 311–327. https://doi.org/10.1017/S0022112099007041.

Kenchington, E., Yashayaev, I., Tendal, O.S., Jørgensbye, H., 2017. Water mass characteristics and associated fauna of a recently discovered Lophelia pertusa (Scleractinia: Anthozoa) reef in Greenlandic waters. Polar Biol. 40, 321–337. https://doi.org/10.1007/s00300-016-1957-3.

Legg, S., Klymak, J., 2008. Internal hydraulic jumps and overturning generated by tidal flow over a tall steep ridge. J. Phys. Oceanogr. 38, 1949–1964. https://doi.org/10.1175/2008jpo3777.1.

Lim, A., Wheeler, A.J., Price, D.M., O'Reilly, L., Harris, K., Conti, L., 2020. Influence of benthic currents on cold-water coral habitats: a combined benthic monitoring and 3D photogrammetric investigation. Sci. Rep. 10, 1–15. https://doi.org/10.1038/s41598-020-76446-y.

MacKinnon, J.A., Zhao, Z., Whalen, C.B., Waterhouse, A.F., Trossman, D.S., Sun, O.M., St Laurent, L.C., Simmons, H.L., Polzin, K., Pinkel, R., Pickering, A., Norton, N.J., Nash, J.D., Musgrave, R., Merchant, L.M., Melet, A.V., Mater, B., Legg, S., Large, W. G., Kunze, E., Klymak, J.M., Jochum, M., Jayne, S.R., Hallberg, R.W., Griffies, S.M., Danabasoglu, G., Chassignet, E.P., Buijsman, M.C., Bryan, F.O., Briegleb, B.P., Barna, A., Arbic, B.K., Ansong, J.K., Alford, M.H., 2017. Climate process team on internal wave-driven ocean mixing. Bull. Am. Meteorol. Soc. 98, 2429–2454. https://doi.org/10.1175/BAMS-D-16-0030.1.

Maier, S.R., Bannister, R.J., van Oevelen, D., Kutti, T., 2020. Seasonal controls on the diet, metabolic activity, tissue reserves and growth of the cold-water coral Lophelia pertusa. Coral Reefs 39, 173–187. https://doi.org/10.1007/s00338-019-01886-6.

Maier, S.R., Kutti, T., Bannister, R.J., van Breugel, P., van Rijswijk, P., van Oevelen, D., 2019. Survival under conditions of variable food availability: resource utilization and storage in the cold-water coral Lophelia pertusa. Limnol. Oceanogr. 64, 1651–1671. https://doi.org/10.1002/lno.11142.

Maier, S.R., Mienis, F., de Froe, E., Soetaert, K., Lavaleye, M., Duineveld, G., Beauchard, O., van der Kaaden, A.-S., Koch, B.P., van Oevelen, D., 2021. Reef communities associated with 'dead' cold-water coral framework drive resource retention and recycling in the deep sea. Deep-Sea Res. Part I Oceanogr. Res. Pap. 175, 103574. https://doi.org/10.1016/j.dsr.2021.103574.

Matos, L., Wienberg, C., Titschack, J., Schmiedl, G., Frank, N., Abrantes, F., Cunha, M.R., Hebbeln, D., 2017. Coral mound development at the Campeche cold-water coral province , southern Gulf of Mexico : implications of Antarctic Intermediate Water increased influence during interglacials. Mar. Geol. 392, 53–65. https://doi.org/10.1016/j.margeo.2017.08.012.

McGrath, T., Nolan, G., McGovern, E., 2012. Chemical characteristics of water masses in the Rockall Trough. Deep. Res. Part I Oceanogr. Res. Pap. 61, 57–73. https://doi.org/10.1016/j.dsr.2011.11.007.

Mienis, F., Bouma, T.J., Witbaard, R., van Oevelen, D., Duineveld, G.C.A., 2019. Experimental assessment of the effects of cold-water coral patches on water flow. Mar. Ecol. Prog. Ser. 609, 101–117. https://doi.org/10.3354/meps12815.

Mienis, F., de Stigter, H.C., de Haas, H., van Weering, T.C.E., 2009. Near-bed particle deposition and resuspension in a cold-water coral mound area at the Southwest Rockall Trough margin, NE Atlantic. Deep. Res. Part I Oceanogr. Res. Pap. 56, 1026–1038. https://doi.org/10.1016/j.dsr.2009.01.006.

Mienis, F., de Stigter, H.C., White, M., Duineveld, G., de Haas, H., van Weering, T.C.E., 2007. Hydrodynamic controls on cold-water coral growth and carbonate-mound development at the SW and SE Rockall Trough Margin, NE Atlantic Ocean. Deep. Res. Part I Oceanogr. Res. Pap. 54, 1655–1674. https://doi.org/10.1016/j.dsr.2007.05.013.

Mienis, F., van Weering, T., de Haas, H., de Stigter, H., Huvenne, V., Wheeler, A., 2006. Carbonate mound development at the SW Rockall Trough margin based on high resolution TOBI and seismic recording. Mar. Geol. 233, 1–19. https://doi.org/10.1016/j.margeo.2006.08.003.

Mohn, C., Rengstorf, A., White, M., Duineveld, G., Mienis, F., Soetaert, K., Grehan, A., 2014. Linking benthic hydrodynamics and cold-water coral occurrences: a high-resolution model study at three cold-water coral provinces in the NE Atlantic. Prog. Oceanogr. 122, 92–104. https://doi.org/10.1016/j.pocean.2013.12.003.

Mohn, C., White, M., 2007. Remote sensing and modelling of bio-physical distribution patterns at porcupine and Rockall bank, northeast Atlantic. Continent. Shelf Res. 27, 1875–1892. https://doi.org/10.1016/j.csr.2007.03.006.

Mortensen, P.B., 2001. Aquarium observations on the deep-water coral lophelia pertusa (L., 1758) (scleractinia) and selected associated invertebrates. Ophelia 54, 83–104. https://doi.org/10.1080/00785236.2001.10409457.

Musgrave, R.C., Pinkel, R., MacKinnon, J.A., Mazloff, M.R., Young, W.R., 2016. Stratified tidal flow over a tall ridge above and below the turning latitude. J. Fluid Mech. 793, 933–957. https://doi.org/10.1017/jfm.2016.150.

O'Reilly, B.M., Readman, P.W., Shannon, P.M., Jacob, A.W.B., 2003. A model for the development of a carbonate mound population in the Rockall Trough based on deep-towed sidescan sonar data. Mar. Geol. 198, 55–66. https://doi.org/10.1016/S0025-3227(03)00094-X.

Orejas, C., Gori, A., Rad-Menéndez, C., Last, K.S., Davies, A.J., Beveridge, C.M., Sadd, D., Kiriakoulakis, K., Witte, U., Roberts, J.M., 2016. The effect of flow speed and food size on the capture efficiency and feeding behaviour of the cold-water coral Lophelia pertusa. J. Exp. Mar. Biol. Ecol. 481, 34–40. https://doi.org/10.1016/j.jembe.2016.04.002.

Penven, P., Debreu, L., Marchesiello, P., McWilliams, J.C., 2006. Evaluation and application of the ROMS 1-way embedding procedure to the central California upwelling system. Ocean Model. 12, 157–187. https://doi.org/10.1016/j.ocemod.2005.05.002.

Pingree, R.D., Griffiths, D.K., 1984. Trapped diurnal waves on porcupine and rockall banks. J. Mar. Biol. Assoc. U. K. 64, 889–897. https://doi.org/10.1017/S0025315400047305.

Purser, A., Larsson, A.I., Thomsen, L., van Oevelen, D., 2010. The influence of flow velocity and food concentration on Lophelia pertusa (Scleractinia) zooplankton capture rates. J. Exp. Mar. Biol. Ecol. 395, 55–62. https://doi.org/10.1016/j.jembe.2010.08.013.

Rowe, G.T., Staresinic, N., 1979. Sources of organic matter to the deep-sea Benthos. Ambio Spec. Rep. 19–23.

Rubenstein, D.I., Koehl, M.A.R., 1977. The mechanisms of filter feeding: some theoretical considerations. Am. Nat. 111, 981–994. https://doi.org/10.1086/283227.

Rüggeberg, A., Dullo, C., Dorschel, B., Hebbeln, D., 2007. Environmental changes and growth history of a cold-water carbonate mound (Propeller Mound, Porcupine Seabight). Int. J. Earth Sci. 96, 57–72. https://doi.org/10.1007/s00531-005-0504-1.

Schulz, K., Soetaert, K., Mohn, C., Korte, L., Mienis, F., Duineveld, G., van Oevelen, D., 2020. Linking large-scale circulation patterns to the distribution of cold water corals along the eastern Rockall Bank (northeast Atlantic). J. Mar. Syst. 212, 103456. https://doi.org/10.1016/j.jmarsys.2020.103456.

Shchepetkin, A.F., McWilliams, J.C., 2005. The regional oceanic modeling system (ROMS): a split-explicit, free-surface, topography-following-coordinate oceanic model. Ocean Model. 9, 347–404. https://doi.org/10.1016/j.ocemod.2004.08.002.

Sherwin, T.J., Read, J.F., Holliday, N.P., Johnson, C., 2012. The impact of changes in North Atlantic Gyre distribution on water mass characteristics in the Rockall Trough. ICES J. Mar. Sci. 69, 751–757. https://doi.org/10.1093/icesjms/fsr185.

Soetaert, K., Mohn, C., Rengstorf, A., Grehan, A., Van Oevelen, D., 2016. Ecosystem engineering creates a direct nutritional link between 600-m deep cold-water coral mounds and surface productivity. Sci. Rep. 6, 1–9. https://doi.org/10.1038/srep35057.

Somoza, L., Ercilla, G., Urgorri, V., León, R., Medialdea, T., Paredes, M., Gonzalez, F.J., Nombela, M.A., 2014. Detection and mapping of cold-water coral mounds and living Lophelia reefs in the Galicia Bank, Atlantic NW Iberia margin. Mar. Geol. 349, 73–90. https://doi.org/10.1016/j.margeo.2013.12.017.

Thiem, Ø., Ravagnan, E., Fosså, J.H., Berntsen, J., 2006. Food supply mechanisms for cold-water corals along a continental shelf edge. J. Mar. Syst. 60, 207–219. https://doi.org/10.1016/j.jmarsys.2005.12.004.

Thorpe, S.A., 2007. An Introduction to Ocean Turbulence. Cambridge University Press.

Titschack, J., Baum, D., de Pol-Holz, R., López Correa, M., Forster, N., Flögel, S., Hebbeln, D., Freiwald, A., 2015. Aggradation and carbonate accumulation of Holocene Norwegian cold-water coral reefs. Sedimentology 62, 1–26. https://doi.org/10.1111/sed.12206.

Ullgren, J.E., White, M., 2010. Water mass interaction at intermediate depths in the southern Rockall Trough, northeastern North Atlantic. Deep. Res. Part I Oceanogr. Res. Pap. 57, 248–257. https://doi.org/10.1016/j.dsr.2009.11.005.

van der Kaaden, A.-S., Mohn, C., van Oevelen, D., 2021. Description accompanying files needed to prepare the Roms-Agrif model for the study by A-S van der Kaaden et al. (DSRP1, 2021), Rockall Bank. NE Atlantic. https://doi.org/10.5281/zenodo.5556805, 10.5281/zenodo.5556805.

van der Kaaden, A.-S., van Oevelen, D., Rietkerk, M., Soetaert, K., van de Koppel, J., 2020. Spatial self-organization as a new perspective on cold-water coral mound development. Front. Mar. Sci. 7, 1–8. https://doi.org/10.3389/fmars.2020.00631.

van der Land, C., Eisele, M., Mienis, F., de Haas, H., Hebbeln, D., Reijmer, J.J.G., van Weering, T.C.E., 2014. Carbonate mound development in contrasting settings on the Irish margin. Deep. Res. Part II Top. Stud. Oceanogr. 99, 297–306. https://doi.org/10.1016/j.dsr2.2013.10.004.

Van Engeland, T., Rune Godø, O., Johnsen, E., Duineveld, G.C.A., van Oevelen, D., 2019. Cabled ocean observatory data reveal food supply mechanisms to a cold-water coral reef. Prog. Oceanogr. 172, 51–64. https://doi.org/10.1016/j.pocean.2019.01.007.

van Haren, H., Mienis, F., Duineveld, G.C.A., Lavaleye, M.S.S., 2014. High-resolution temperature observations of a trapped nonlinear diurnal tide influencing cold-water corals on the Logachev mounds. Prog. Oceanogr. 125, 16–25. https://doi.org/10.1016/j.pocean.2014.04.021.

van Oevelen, D., Duineveld, G., Lavaleye, M., Mienis, F., Soetaert, K., Heip, C.H.R., 2009. The cold-water coral community as a hot spot for carbon cycling on continental margins: a food-web analysis from Rockall Bank (northeast Atlantic). Limnol. Oceanogr. 54, 1829–1844. https://doi.org/10.4319/lo.2009.54.6.1829.

Vic, C., Naveira Garabato, A.C., Green, J.A.M., Waterhouse, A.F., Zhao, Z., Melet, A., de Lavergne, C., Buijsman, M.C., Stephenson, G.R., 2019. Deep-ocean mixing driven by small-scale internal tides. Nat. Commun. 10 https://doi.org/10.1038/s41467-019-10149-5.

Wagner, H., Purser, A., Thomsen, L., Jesus, C.C., Lundälv, T., 2011. Particulate organic matter fluxes and hydrodynamics at the Tisler cold-water coral reef. J. Mar. Syst. 85, 19–29. https://doi.org/10.1016/j.jmarsys.2010.11.003.

Wang, H., Lo Iacono, C., Wienberg, C., Titschack, J., Hebbeln, D., 2019. Cold-water coral mounds in the southern Alboran Sea (western Mediterranean Sea): internal waves as an important driver for mound formation since the last deglaciation. Mar. Geol. 412, 1–18. https://doi.org/10.1016/j.margeo.2019.02.007.

Wheeler, A.J., Beyer, A., Freiwald, A., de Haas, H., Huvenne, V.A.I., Kozachenko, M., Olu-Le Roy, K., Opderbecke, J., 2007. Morphology and environment of cold-water coral carbonate mounds on the NW European margin. Int. J. Earth Sci. 96, 37–56. https://doi.org/10.1007/s00531-006-0130-6.

White, M., Dorschel, B., 2010. The importance of the permanent thermocline to the cold water coral carbonate mound distribution in the NE Atlantic. Earth Planet Sci. Lett. 296, 395–402. https://doi.org/10.1016/j.epsl.2010.05.025.

White, M., Roberts, J.M., van Weering, T., 2007. Do bottom-intensified diurnal tidal currents shape the alignment of carbonate mounds in the NE Atlantic? Geo Mar. Lett. 27, 391–397. https://doi.org/10.1007/s00367-007-0060-8.

Wienberg, C., Titschack, J., Frank, N., De Pol-Holz, R., Fietzke, J., Eisele, M., Kremer, A., Hebbeln, D., 2020. Deglacial upslope shift of NE Atlantic intermediate waters controlled slope erosion and cold-water coral mound formation (Porcupine Seabight, Irish margin). Quat. Sci. Rev. 237, 106310. https://doi.org/10.1016/j.quascirev.2020.106310.

Wienberg, C., Titschack, J., Freiwald, A., Frank, N., Lundälv, T., Taviani, M., Beuck, L., Schröder-Ritzrau, A., Krengel, T., Hebbeln, D., 2018. The giant Mauritanian cold-water coral mound province: oxygen control on coral mound formation. Quat. Sci. Rev. 185, 135–152. https://doi.org/10.1016/j.quascirev.2018.02.012.

Wu, L., Miao, C., Zhao, W., 2013. Patterns of K1 and M2 internal tides and their seasonal variations in the northern South China Sea. J. Oceanogr. 69, 481–494. https://doi.org/10.1007/s10872-013-0183-7.